LTCC TECHNOLOGY FOR SATELLITE COMMUNICATION AT KA-BAND

Christian Friesicke, Sascha Brosius, Torben Baras, Alexander Molke, and Arne F. Jacob
Inst. für Hochfrequenztechnik, Hamburg Univ. of Technology, 21073 Hamburg, Germany,
Tel: +49 40 42878-3370, Fax: +49 40 42878-2755, email: christian.friesicke@tuhh.de

Abstract

This paper presents a satellite transponder system based on LTCC technology for applications at Ka-band. The transponder system is one of many experimental payloads onboard the TET-1 experiment carrier of the German Aerospace Agency. LTCC technology is advantageous for designing modules and subsystems especially for radio frequency (RF) applications. By means of hybrid integration circuit functionality can be shifted from expensive semiconductors to the inexpensive ceramic. Additionally, the ceramic multilayer can function as a chip packaging solution. In this fashion, various modules have been fabricated and connected together as a transparent satellite transponder. This transponder passed all mechanical, thermal and electromagnetic compatibility tests and is currently integrated into the payload segment of the satellite TET-1, which is scheduled for launch in the second half of 2011.

1. INTRODUCTION AND KERAMIS PROJECT

The project KERAMIS (Ceramic Microwave Circuits for Satellite Communications) is a cooperation between industrial and academic partners. Its goal is to improve the technology readiness level of low-temperature co-fired ceramic (LTCC) technology for space applications, particularly for future Ka-band satellite communication systems, which operate at a downlink frequency of about 20 GHz. Within the project, three different experiments were developed, each of which contains circuit building blocks based on LTCC technology and operated at the 20 GHz downlink band: an experiment containing an LTCC switch matrix [1,2] was designed at *Ilmenau University of Technology*, an experiment comprising a fractional-N synthesizer, amplifiers, switches, and power detectors integrated in LTCC [3,4] was developed by *IMST GmbH*, and a transponder experiment based on LTCC synthesizers, amplifiers, mixers, and power detectors [5,6] was designed by the authors. The ultimate goal of the project is to run these experiments in space, thus verifying their functionality on-orbit. To reach this goal, the KERAMIS project was granted permission to fly the hardware as one of eleven payloads onboard the small scientific satellite TET-1. The three experiments are assembled into one box, which forms the KERAMIS payload. The mechanical design and integration of this payload box was handled by our partner *Astro- und Feinwerktechnik Adlershof GmbH* in Berlin [7].

This paper discusses the transponder experiment and is structured as follows: in Section 2, the basic process flow of LTCC technology and the capabilities of the used LTCC process are explained, after which we present the most important LTCC modules that are utilized in our experiment. Section 3 illustrates the basic transponder topology by means of block diagrams and focuses on the concepts used for a redundant design. The model philosophy is briefly outlined, and some of the most recent experimental results of the protoflight model (PFM) of our transponder are presented in Section 4. The last Section 5 deals with on-orbit verification, describing the different experimental setups, by which the correct operation of our LTCC-based transponder is verified.

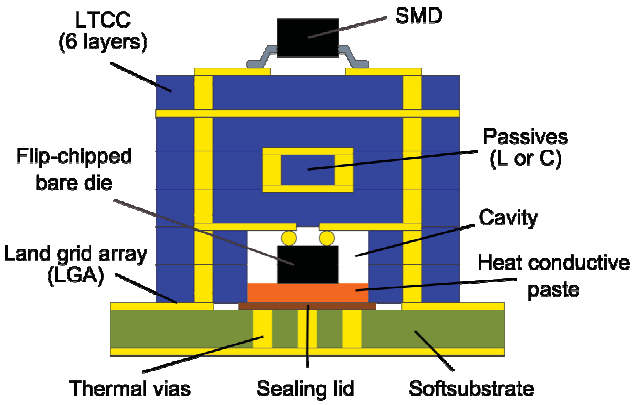

Fig. 1. Example of circuit design features available through the LTCC ceramic multilayer process.

2. LTCC-TECHNOLOGY AND -MODULES

LTCC is a technology for the fabrication of ceramic multilayer circuits. “Co-fired” refers to the characteristic feature of the process, by which all metallic and dielectric layers are sintered together in one step. The term “low-temperature” means that the sintering temperature profile stays below 1000 ℃, which means that a broader ran ge of materials are compatible with the process (e.g., gold metallization).

The main advantages of LTCC are the good material properties of the ceramic at microwave frequencies and its process features, which enable the design of compact and light weight circuits especially suited for operation in space.

Examples for advantageous material properties are the good conductivity of the gold and silver layers and the low dielectric loss up to millimeter-wave frequencies. In contrast to conventional printed circuit boards the ceramic has a good thermal conductivity and is both thermally and chemically stable. The latter is especially important for the utilization of LTCC in harsh environments.

Some of the advantages in terms of process features are the fine-line pattering (down to 50µm lines/spaces) of RF structures and the possibility to embed passive

components (planar inductors, thick-film capacitors, and thick-film resistors) into the multilayer substrate, which is shown in Fig. 1. Another key feature is the ability to create cavities (i.e., cutouts inside some of the layers). Such cavities are useful for the placement of monolithically integrated microwave circuits (MMICs) or discrete transistors in the form of bare dies. The cavity may then be hermetically sealed by brazing a Kovar lid on top of it. The possibility to completely enclose sensitive semiconductor devices inside a hermetically sealed ceramic module makes LTCC ideal for space applications: the technology offers a solution to combine multilayer circuit design with package design.

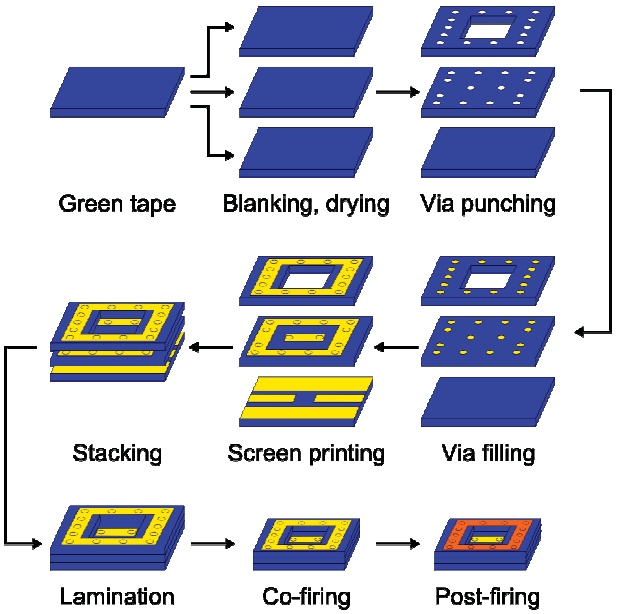

Fig. 2. Sequence of steps required for the fabrication of LTCC ceramic multilayer circuits.

The fabrication of LTCC modules is accomplished in multiple steps as depicted in Fig. 2. The base material of LTCC is available as "green tape" from several suppliers [19-22] and is usually delivered on rolls. As a first step, the tape is flattened on a clean stainless steel table. Further preparation of the green tape includes cutting and drying at 120 ℃ for 5 to 30 min. In the following, each layer of the multilayer setup is processed in parallel. This processing starts with punching the vias and cavities into the tape. There are different punching tools available for different via diameters (e.g., 50 µm thin vias for densely packed interconnects, or 200 µm thick vias for thermal vias). The cavities are cut out by punching their outline with a thin tool, which enables almost arbitrary shapes.

The vias are filled with silver or gold conductive paste. Subsequently, the metal layers on top of the green tape are printed by a silk-screen process: using a squeegee, the cofireable, conductive paste is passed through a fine wire screen. All layers are then optically inspected before they are stacked, so that nonconforming units may be replaced. The following stacking process is done by using mechanical alignment pins. It may result in a layer misalignment of up to 20 µm. Following that, the stacked LTCC is laminated by applying several Bars of pressure at, for example, 70 ℃ during 10 min. After laminati on, the complete stackup is sintered for a few hours using an appropriate temperature profile. The organic components of the green tape burn out at a temperature of about 450 ℃, which is then raised to approximately 850 ℃ fo r about 10 min. Some materials, such as solderable pastes, need to be printed onto the LTCC after co-firing. The second firing is called post-firing, and its temperature profile depends on the used materials and can vary in a wide range.

The cross-section of the LTCC module in Fig. 1 also shows a special packaging approach for power applications: inside the cavity a bare die is flip-chipped onto an inner layer of the module. The cavity is sealed by a lid, which also functions as a heat sink [8]. In this case, the short primary thermal path through the heat conductive paste and lid down to the soft substrate results in smaller thermal resistance in contrast to the standard method, which employs thermal vias. The side opposite to the cavity can be used to solder surface mountable devices (SMD) onto the LTCC. In this way, additional hardware can be installed, for example, as control circuitry for the LTCC module. These features allow the design of complex, yet compact microwave modules, also in lower power applications such as in synthesizers or mixers. When mounted onto the soft substrate, the LTCC modules can also be processed like SMD components.

Proper signal transfer between LTCC module and motherboard with low reflection or attenuation loss is important in order to maintain the interior circuit performance. The so-called second-level interconnect between soft substrate and module is thus a very important building block which may be used for all microwave signal ports in all modules. An early design study [9] showed that land grid arrays (LGAs) with low loss can be design for broadband signals, which is because of their shorter transmission paths and reduced parasitics, compared to interconnects realized by wire bonding. Furthermore, the designed LGAs are mechanically and thermally robust interconnects [10] and thus well suited for space applications.

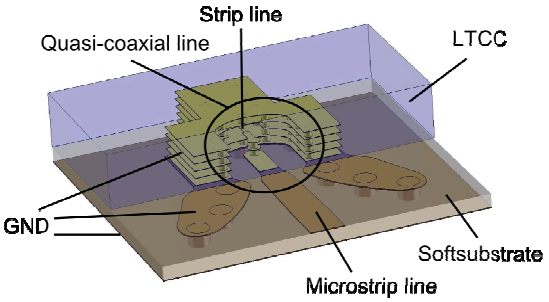

Fig. 3. Three-dimensional view of the designed land-grid array mounted on top of a soft substrate.

Fig. 3 shows a three-dimensional view of the LGA second-level interconnect structure. It starts on the soft substrate with a microstrip line which is transformed into a tapered coplanar line by gradually decreasing distance to ground. This is followed by a vertical section in which the signal propagates upwards on a quasi-coaxial line. At the end of this line, the signal propagates again in the horizontal direction along a shielded stripline structure. The characteristic impedance of each transmission line section is optimized to 50 Ohm in order to minimize

reflections. This behavior can be seen from simulated data of reflection and transmission coefficients in Figs. 4 and 5, respectively. High transmission and low reflection is obtained from DC to approximately 40 GHz, thus making the second-level interconnect usable up to the Ka-Band. At higher frequencies there is an undesired drop in transmission, which is caused by the excitation of higher-order modes.

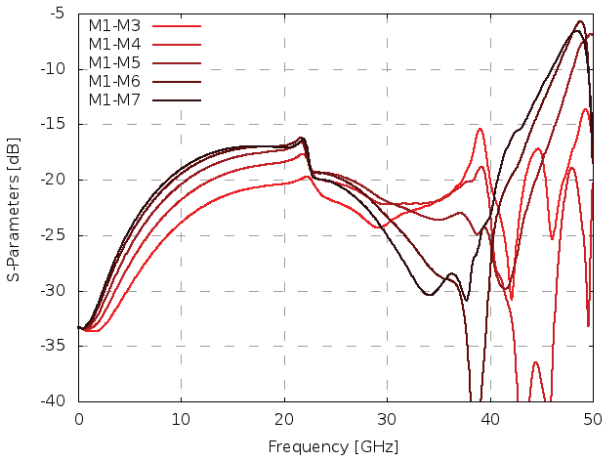

Fig. 4. Simulated reflection coefficient at the input of the LGA structure in dB versus frequency plotted for signal transitions from layer 1 to layers 3-7.

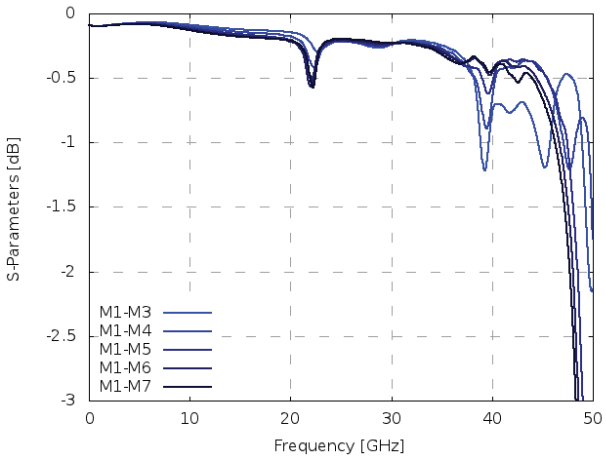

Fig. 5. Simulated transmission coefficient from the input (at the soft substrate) to the output (inside the LTCC module) in dB versus frequency plotted for signal transitions from layer 1 to layers 3-7.

The above described concept of using LGAs and a standard surface-mount process for soldering the LTCC modules onto a high frequency soft substrate was applied in the design of a transparent transponder. In the following, the LTCC RF modules, which form the core of the transponder, namely, synthesizer, mixer, medium power amplifier, and power detector modules, are described along with their most important performance figures. All modules operate at the K-Band downlink frequency of 20 GHz. They were manufactured by our partner *MSE* in Berg, Oberfranken [11].

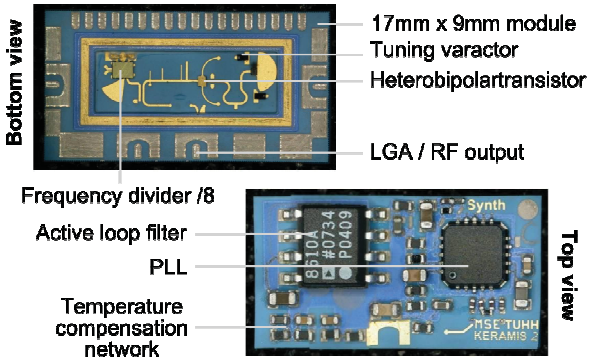

Fig. 6. Bottom and top view of the fabricated LTCC synthesizer module with temperature compensation.

The synthesizer module is depicted in Fig. 6. It has a compact size of 9x17 mm² and uses a GaAs hetero-junction bipolar transistor (HBT) as active element [12]. The generated RF output signal has a power of approximately 7 dBm at 20 GHz. In addition, the frequency is stabilized with an integrated phased-locked loop (PLL). Due to the unavailability of PLLs operating directly at K-band an external divider-by-eight is employed and used with a commercially available PLL chip at 2.5 GHz. A frequency tuning range of 19.5 GHz to 20.1 GHz is achieved with a substrate-integrated resonator, which is tunable by means of a varactor diode. In Fig. 7 the output spectrum is depicted. The phase noise is measured as -118 dBc/Hz at 1 MHz offset frequency. Furthermore, a temperature compensation was added [13] to provide robust operation even with the expected higher temperature variations in space.

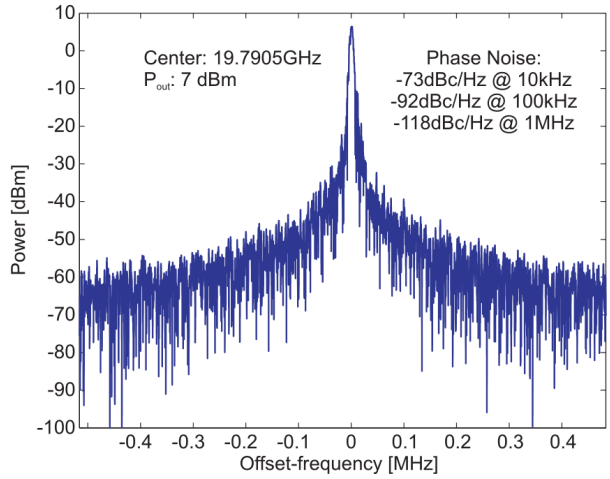

Fig. 7. Measured output spectrum and phase noise of the LTCC synthesizer module.

As explained later in Section 3, our experiment does not communicate directly at 20 GHz with the ground station. Instead, it uses the frequencies from telecommand and telemetry of the satellite, which are 2.0 GHz and 2.2 GHz, respectively. Since all modules operate at K-Band, a frequency mixer is needed to translate the input signal of our experiment to K-band and, once processed by the transponder chain, again back to S-band. To this end, a series of mixer modules (singly balanced and doubly balanced) were designed [14-16]. The singly balanced mixer in Fig. 8 was chosen as best suited for our

applications. Its size is about 8x9 mm², and the module offers a good conversion loss of 8 dB and requires low local oscillator (LO) power. The exploded view in Fig. 8 shows that RF and LO signals are fed into a rat-race ring coupler. The other two (inner) ports of the ring are connected to anti-parallel Schottky diodes. The converted intermediate frequency (IF) signal is tapped between the diodes and fed through a via hole where it is connected to a circularly bent lowpass filter. The conversion loss between the RF signal at approximately 20 GHz and the converted IF signal at approximately 2 GHz is shown in Fig. 9. The operating range is limited to 20 GHz to 22 GHz, which is sufficient for our purposes.

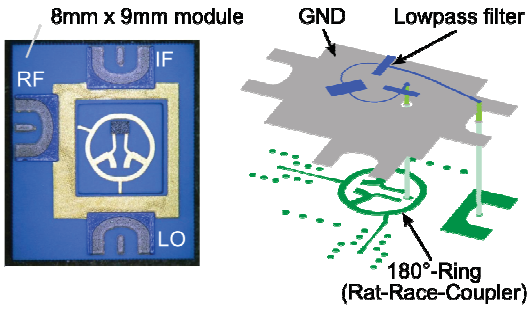

Fig. 8. Bottom view of the LTCC mixer module with flip-chipped Schottky diode inside the cavity (left); exploded view of the module (right).

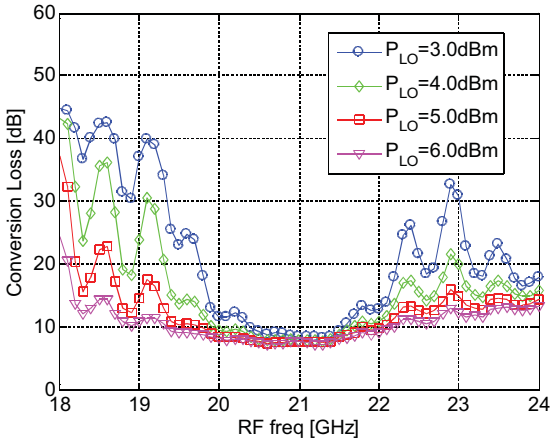

Fig. 9. Measured conversion loss in dB versus RF frequency for 2 GHz IF frequency.

The third LTCC module for on-orbit verification is the medium power amplifier (MPA) depicted in Fig. 10. This module has an outline dimension of about 10x11 mm². At the bottom, a double layer of Kovar material is used as a sealing lid. The thick sealing lid is placed into a cutout of the soft substrate, thereby creating a direct thermal connection to the aluminum carrier, onto which the soft substrate is glued. At the top, surface-mount components are used to implement active bias circuitry. The MPA is based on a commercially available chip and features an output power of 0.3 Watt to 0.5 Watt (saturated output power) along with a gain of about 20 dB (cf. Fig. 11) and 25% power-added efficiency.

The last LTCC module used in our experiment is a power detector module operating at K-band. It is used to monitor the input and output power of the medium power amplifier, and hence, it may also monitor the amplifier's gain.

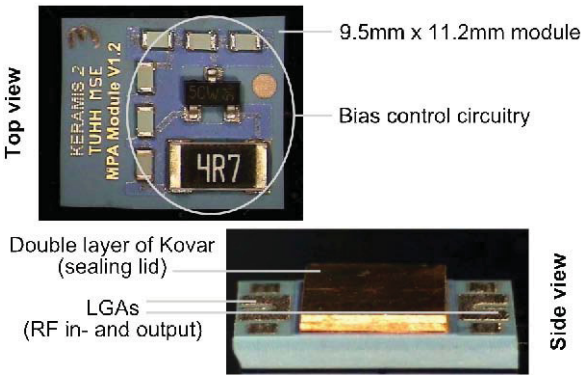

Fig. 10. Top view of the MPA module with active bias control (top); side view showing the double Kovar layer (bottom).

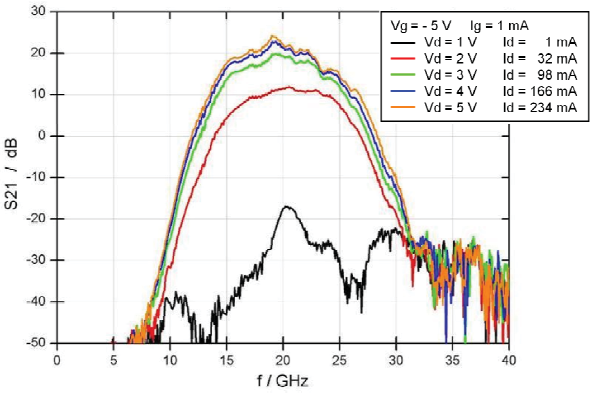

Fig. 11. Measured gain of the MPA module at different drain bias levels.

3. TOPOLOGIES FOR SATELLITE TRANSPONDER SYSTEMS

In future Ka-band satellite systems, the Ka-band uplink signal at 30 GHz is translated to a K-band signal at 20 GHz. Our experiment differs from this scenario because, firstly, licensing the required spectrum is complicated and expensive, and secondly, the downlink power budget would require a traveling-wave tube amplifier (TWTA), which is too heavy and bulky for the scientific satellite TET-1. Instead, in our on-orbit experiment we use the same frequencies as the satellite telemetry and telecommand signaling unit for up- and downlink at 2.0 and 2.2 GHz, respectively. Fig. 12 illustrates this concept: the orange building blocks are components operating at K-band, and the blue building blocks are S-band components. From an external point of view, our payload behaves as transparent S-band transponder. Inside, the signal first passes a transmit-/receive duplex filter, is then amplified and upconverted to K-band (by mixer Mix1 and oscillator LO1), filtered, and finally downconverted to S-band (by mixer Mix2 and oscillator LO2). Fig. 12 shows a basic diagram without MPA module or power detectors; however, these may be inserted in the signal path between the up- and downconverters. The most important result – successful operation of the K-band LTCC modules – may hence be demonstrated by the frequency conversion from S-band to K-band and back to S-band.

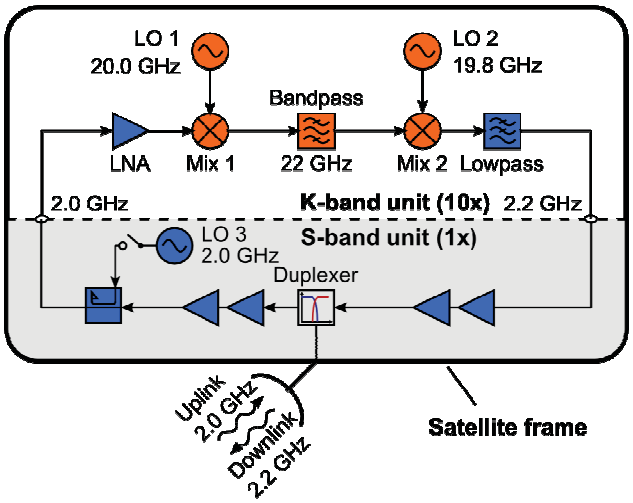

Fig. 12. Block diagram of the auxiliary S-band system (blue) and a simple LTCC transponder path (orange).

Redundant design is a requirement for the experimental payload. To this end, the payload consists of two boards, which also offer different degrees of redundancy. Board1 (called the “nominal” board) is shown in Fig. 13 and has a two-fold redundancy: it consists of two signal branches, which can be independently activated by switching on the low-noise amplifier (LNA) at the respective branch input. The branch in the lower part of Board1 is exactly as in the block diagram of Fig. 12. The branch in the upper part of Board1 is more complex. It contains a MPA module with power detectors and couplers at the input and output. The couplers added before and after the amplifier result in a unity net gain so as to maintain the same signal levels as in the first branch. The direct output signals of the couplers are additionally used for on-board signal monitoring with power detectors.

Board2 (called the “redundant” board) is also depicted in Fig. 13. It also has two branches but these are not as clearly separated as in Board1. Again, there is a lower and an upper branch, which is selected by biasing the desired amplifier at the input. Here, the upper branch is the simple version of Fig. 12 consisting only of a bandpass filter between up- and downconverter. The lower branch is the more complex version with MPA module, couplers, and power detectors. Between the up- and downconverter mixers, the two branches are exactly as on Board1. What differs is the way in which the mixers are driven regarding the local oscillator signal distribution. There are four synthesizer modules: the two on the right are connected to a 3 dB coupler, so that each of the synthesizers may be used to feed the upconverter mixers. Similarly, the two synthesizers on the left are connected to the downconverter mixers via a 3 dB coupler. Board2 thus offers two branches, two synthesizers for the upconverter, and two synthesizers for the downconverter, resulting in eight different ways in which the board can be operated. The advantage of this topology is that even if one of the upconverter synthesizers and/or one of the downconverter synthesizers fails, the board is still fully operational. On the downside, the power of the synthesizers is split by the coupler, so that only half of the power arrives at the mixer of the activated branch. As can be seen from Fig. 9, the local oscillator power has an impact on the conversion loss, which is degraded for lower LO power.

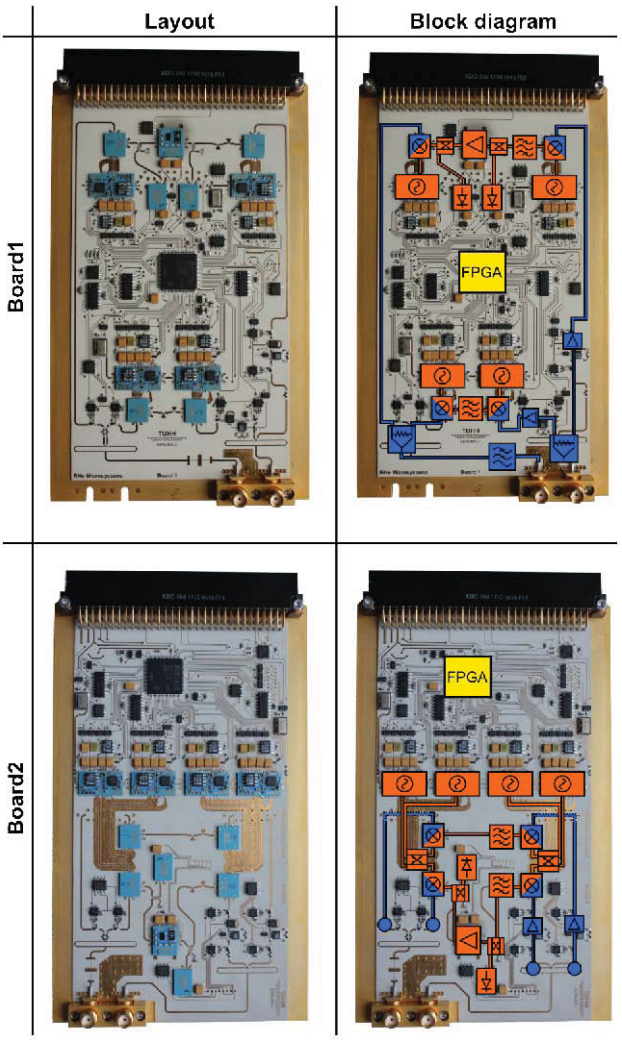

Fig. 13. Board layout (left column) and overlaid block diagram (right column) of Board1 (top row) and Board2 (bottom row).

Both boards are controlled by an individual field-programmable gate array (FPGA), which is used to switch components on or off, thereby also selecting which of the two configurations (determined by the branch) is activated in Board1, or which of the eight configurations (determined by the branch and synthesizers) is activated in Board2. In total, the transponder offers 2+8 = 10 configurations. The hardware is complemented by temperature sensors (four on each board), which are read out via a one-wire bus and sense the temperature at different places, for example, in close proximity to the medium power amplifier modules.

4. MODEL PHILOSOPHY AND TESTING

Within the KERAMIS project, the following model philosophy was pursued: two technology models (TM1 and TM2), a structural-thermal model (STM), an engineering model (EM), and a protoflight model (PFM) were constructed and subjected to the required mechanical, thermal, or electromagnetic stress tests.

The models TM1 and TM2 were constructed to verify that the used methods for assembly, integration, and

packaging are suitable for the intended operation in space. In these models, ultrasonic bonding, thermosonic bonding, and thermocompression bonding were compared for wire bonds and flip-chip assembly. During vibrational tests, there were failures associated with flip-chipped dies using ultrasonic bonding. Consequently, thermocompression bonding was chosen as preferred method for flip-chip assembly, and thermosonic bonding was used for setting wire bonds or placing stud bumps. Furthermore, the mechanical stability of the soldered LGA interconnects was improved by changing from our in-house reflow soldering process with SnPb alloys to the process of our project partner *RHe Microelectronics* (now *Cicor*) [17] using an SnPbAg alloy.

While the STM is only a dummy with the same mechanical and thermal properties as the real payload, the EM was built according to form, fit, and function of the final payload. The advantage of this approach is the reduced risk during the testing of the protoflight model. This is important because the protoflight model is not only the last model which is tested but also the payload which is intended to be launched.

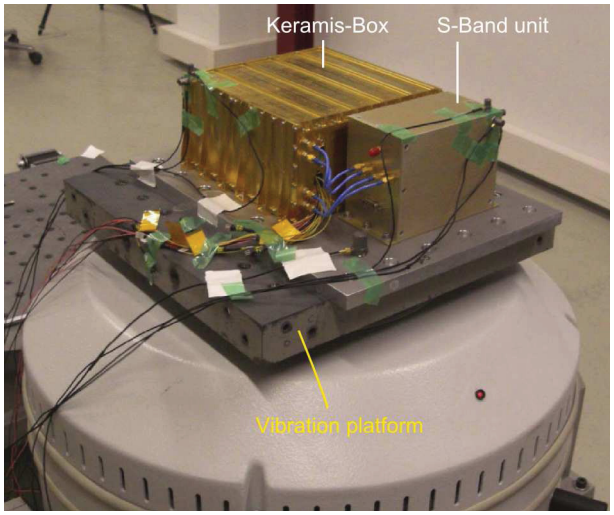

Fig. 14. KERAMIS PFM payload setup for vibrational tests.

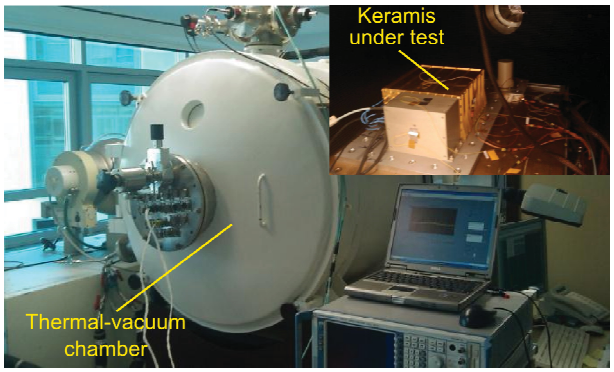

Fig. 15. Thermal-vacuum chamber at the German Aerospace Center, Berlin; KERAMIS PFM payload inside the chamber (inlay).

Successful environmental testing of the PFM is thus mandatory in order to get permission to fly the hardware onboard the satellite. Along with the two other KERAMIS experiments our transponders were subjected to mechanical, thermal, and electromagnetic compatibility tests. Vibrational tests, for example, simulate the conditions during rocket launch, and thermal-vacuum tests mimic the environmental conditions in orbit. Fig. 14 shows the setup for vibrational tests: the KERAMIS box along with the auxiliary S-band Tx/Rx unit from Fig. 12 is mounted on a metal carrier which is attached to a vibration platform. Vibration is applied to all three axes as sinusoidal and random excitation. In addition, half-sinusoidal shocks tests were applied. Fig. 15 shows the thermal-vacuum chamber and the payload within the chamber. The temperature is varied between -20 ℃ a nd 50 ℃ during thermal cycling. Both vibrational and thermal-vacuum tests were undertaken by our partner *Astro- und Feinwerktechnik* at the facilities of the *German Aerospace Agency* in Berlin-Adlershof. Further electromagnetic compatibility (EMC) tests were carried out by our partner *Kayser-Threde* [18]. All required tests were passed by the KERAMIS payload.

Measurement data obtained during vibrational and thermal-vacuum tests is exemplarily depicted in Fig. 16: the plot shows the power levels detected at different points in the transponder signal path. The black horizontal bars mark the specified pass-/fail-boundary. As can be seen from the abscissa, the experiment was run thirty times, where six runs were due to vibrational tests, 18 runs were due to thermal cycling, and the remaining runs were functional tests conducted before, between, and after vibrational and thermal-vacuum tests. In addition to the power detectors, we also recorded onboard voltages and temperatures. Finally, the overall functionality of our payload was successfully verified by measuring the transponder's output spectrum shown in Fig. 17: the time-series of the output spectrum exhibits ten distinct time intervals where power is generated. This number (ten) comes from the eight redundant combinations of Board2 and two redundant combinations of Board1 which are run during one experiment. Left and right to the main peaks one can also see spurious intermodulation peaks at offset frequencies of 10 MHz and 20 MHz. These peaks are due to an internal frequency hopping scheme in which the synthesizers are periodically programmed. The spurious signals could be easily suppressed by programming the synthesizers in a different way. In our case they are desired because they allow us to observe the periodic programming of the synthesizers in real-time.

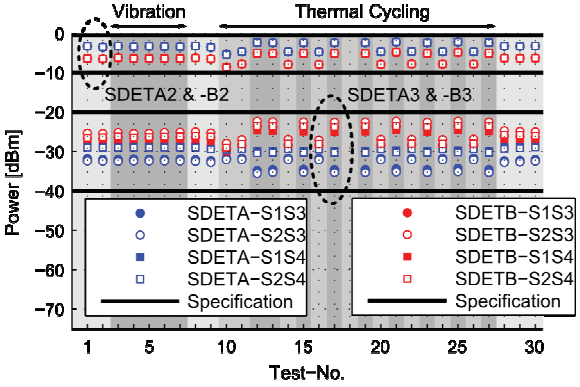

Fig. 16. Power levels measured by the S-band power detectors at different points in the transponder chain.

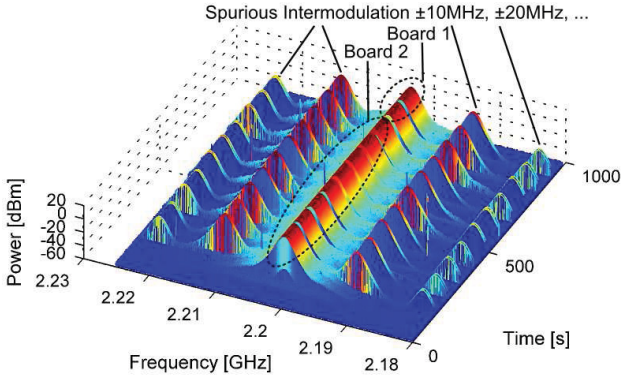

Fig. 17. Time-series of measured output spectra of the transponder experiment.

5. LINK BUDGET AND OPERATIONAL MODES

The satellite TET-1 is expected to be launched in the second half of 2011 and will reach an orbit of 550 km. One orbit lasts about 90 min while direct communication via a line of sight (LOS) link with the ground station in Weilheim, Germany, will only be available for approximately 10 min. Fig. 18 shows the most relevant system parameters that are important for the signal transmission between TET-1 and the ground station. A link budget analysis was carried [5] out to decide which antenna size provides a stable link with sufficient signal-to-noise ratio (SNR) during overflight. As can be seen from the simulated result in Fig. 19 the 15 meter dish in Weilheim always results in more than 20 dB SNR.

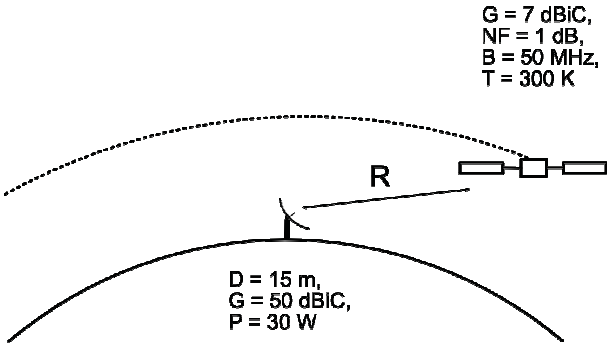

Fig. 18. System parameters for LOS link between TET-1 and the ground station in Weilheim.

Our experiment provides two operational modes. In the first mode the experiment works as transponder: it receives an external signal and transmits it back to the downlink, thus requiring LOS conditions. The main advantage of this operational mode is the possibility to record a time-series of output spectra similar to that shown in Fig. 16.

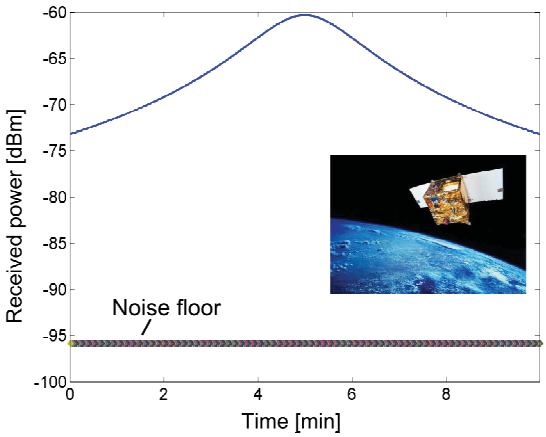

Fig. 19. Simulated link budget analysis for LOS link between TET-1 and the 15 m dish in Weilheim.

The second mode is intended for endurance tests under non-LOS conditions: here the external signal is simulated by an internal oscillator (LO3 in Fig. 11). The signal is then passed through the entire transponder chain with the transmitter being switched off. The internal oscillator may also be used during LOS conditions, for example, when there is no uplink signal available. The endurance test's main purpose is to exert thermal stress, which is especially critical for the MPA modules. In this way, we intend to demonstrate the usefulness of the chosen packaging approach for the power modules.

6. CONCLUSION

Key features of LTCC technology, which are most relevant for the design of space-qualified RF modules, are presented along with features, which are advantageous for fabrication of highly integrated subsystems. A selection of RF modules designed in LTCC is shown along with their most important performance figures. From these subsystems two redundant transponder boards are constructed and tested successfully under certain environmental influences. Finally, we discuss the methods used to verify the correct operation of our experiment on orbit.

7. ACKNOWLEDGMENT

The authors wish to acknowledge funding and support of this work by the *German Aerospace Center* (DLR) on behalf of the *German Federal Ministry of Economics and Technology* (BMWi) under research contracts 50YB0314 and 50YB0623.

8. REFERENCES

[1] S. Humbla, K.-H. Drüe, R. Stephan, D. Stöpel, J. F. Trabert, G. Vogt, M. A. Hein, "Qualification of a compact Ka-Band Switch Matrix for On-Orbit-Verification," 3rd German Microwave Conference (GeMiC2008), Hamburg, Germany, March 10-12, 2008, pp. 454-457.

[2] S. Humbla, J. Müller, R. Stephan, D. Stöpel, J. F. Trabert, G. Vogt, M. A. Hein, "Reconfigurable Ka-Band Switch Matrix for On-Orbit Verification," 39th European Microwave Conference (EuMC2009), Rome, Italy, Sept. 29 - Oct. 1, 2009, pp. 610-613.

[3] R. Kulke, G. Moellenbeck, C. Guenner, P. Uhlig, and M. Rittweger, "LTCC Multi-Chip Modules for Ka-Band Multimedia Satellite Technology," 3rd German Microwave Conference (GeMiC2008), Hamburg, Germany, March 10-12, 2008, pp. 450-453.

[4] M. Rittweger, R. Kulke, R. Follmann, and I. Wolff, "Innovative Technologies for RF Circuitry in Satellite Payload," 3rd European Conference on Antennas and Propagation (EuCAP2009), Berlin, Germany, March 23-27, 2009, pp. 484-486.

[5] T. Baras, S. Brosius, and A. F. Jacob, "K-Band/S-Band Satellite Transponder System for On-Orbit Evaluation of LTCC Technology," 5th European Radar Conference (EuRAD2008), Amsterdam, The Netherlands, October 30-31, 2008, pp. 348-351.

[6] S. Brosius, C. Friesicke, T. Baras, A. Molke, and A. F. Jacob, “Satellite Transponder System with Multiple Redundancy for On-Orbit Verification of LTCC Technology at K-Band,“ 41st European Microwave Conference (EuMC2011), Manchester, United Kingdom, October 10-13, 2011, accepted for publication.

[7] Astro- und Feinwerktechnik Adlershof GmbH, Berlin.
Online: http://www.astrofein.com/

[8] T. Baras and A. F. Jacob, “Thermal Packaging Concept for LTCC Microwave Power Applications,” 3rd German Microwave Conference (GeMiC2008), Hamburg, Germany, March 10-12, 2008, pp. 446-449.

[9] T. Baras and A. F. Jacob, “Advanced Broadband 2nd-Level-Interconnects for LTCC Multi-Chip-Modules,” 1st German Microwave Conference (GeMiC2005), Ulm, Germany, April 5-7, 2005, pp. 21-24.

[10] T. Baras, C. M. Hernández, and A. F. Jacob, “Electrical and Thermomechanical Evaluation of 2nd-Level-Interconnects for LTCC Modules,” 39th International Symposium on Microelectronics (IMAPS2006), San Diego, California, USA, October 8-12, 2006, pp. 1142-1147.

[11] Micro Systems Engineering GmbH, Berg/Oberfr.
Online: http://www.mse-microelectronics.de/

[12] T. Baras and A. F. Jacob, "Vertically Integrated Voltage-Controlled Oscillator in LTCC at K-Band," IEEE MTT-S International Microwave Symposium Digest, Atlanta, Georgia, USA, June 15-20, 2008, pp. 359-362.

[13] T. Baras, and A. F. Jacob, "Temperature Drift Compensation Technique for a Hybrid LTCC Oscillator at 20 GHz," 4th European Microwave Integrated Circuits Conference (EuMIC2009), Rome, Italy, September 28-29, 2009, pp. 467-470.

[14] T. Baras, J. Müller, and A. F. Jacob, "K-Band LTCC Star Mixer with Broadband IF Output Network," IEEE Transactions on Microwave Theory and Techniques, vol. 55, no. 12, pp. 2766-2772, December 2007.

[15] T. Baras and A. F. Jacob, "Integrated LTCC Synthesizer and Signal Converter Modules at K-Band," IEEE Transactions on Microwave Theory and Techniques, vol. 57, no. 1, pp. 71-79, Januar 2009.

[16] T. Baras and A. F. Jacob, "Multilayer-Integration of Wideband LTCC Image Rejection Mixers at K-band," 6th German Microwave Conference (GeMiC2010), Berlin, Germany, March 15-17, 2010, pp. 86-89.

[17] Cicor Microelectronics, RHe Microsystems GmbH, Radeberg.
Online: http://www.cicor.com/

[18] Kayser-Threde GmbH, Munich.
Online: http://www.kayser-threde.com/

[19] DuPont, Wilmington, DE, USA.
Online: http://www.dupont.com/

[20] Heraeus Holding GmbH, Hanau.
Online: http://www.heraeus.de/

[21] ESL ElectroScience, King of Prussia, PA, USA.
Online: http://www.electroscience.com/

[22] Ferro Corporation, Cleveland, OH, USA.
Online: http://www.ferro.com/